Article

Journal of Vibration and Control
2024, Vol. 30(1-2) 156–168

DOI: 10.1177/10775463221142663
journals.sagepub.com/home/jvc
Sage

Improving performance of a nonlinear absorber applied to a variable length pendulum using surrogate optimization

Oleg Gaidai[1], Yu Wu[1], Ivan Yegorov[2], Panagiotis Alevras[3], Junlei Wang[4], and Daniil Yurchenko[5]

Abstract

The paper investigates a nonlinear vibration mitigation strategy of a variable length pendulum subjected to a harmonic external excitation. A nonlinear absorber in a form of a tri-pendulum system is used to reduce the response of the primary pendulum. Thus, the paper investigates a non-stationary problem of nonlinear vibration mitigation of the primary pendulum using another nonlinear passive pendulum absorber. Due to genuine interest in capturing the nonlinear dynamic interaction, the paper numerically studies the performance of the primary mass and absorber, first, by constructing 2D maps in the unrestrained parametric space, which demonstrate the qualitative behavior of the system. Then, the surrogate optimization technique is used to tune the absorber's parameters within a given bounded set of parameters' values. The optimization is conducted based on a priori known reeling speed or acceleration/deceleration of the primary pendulum, thereby completely removing the need for acquiring a current system states essential for active feedback control. The obtained numerical results validate the proposed strategy and demonstrate high performance of the nonlinear passive absorber when it is properly tuned.

Keywords

Crane's payload vibration, passive nonlinear absorber, nonlinear energy sink, pendulum absorber, pendulum vibration mitigation, surrogate optimization

1. Introduction

Various mechanisms for lifting goods, similar to cranes, have been serving humans for thousands of years.

There are currently no systems that allow cranes to operate autonomously no matter how perfect the weather conditions are. One of the reasons is the unpredictability of the surrounding environment, which together with the motion of the crane and payload may result in adverse swinging vibrations of the payload. These vibrations, if not mitigated, can lead to a collision between the payload and the surrounding structures, increase in the hoist tension leading to its failure, or result in the collapse of the crane itself due to unbalance. Thus, these vibrations should be mitigated well in advance, which is a nontrivial task for an inexperienced operator. The reason is that these vibrations occur in the horizontal plane, whereas the operator can control the motion of the payload in the perpendicular vertical direction. This is a challenging control problem, which has been attracting significant interest from researchers all over the world.

Cranes can be classified by the degrees of freedom they have (Abdel-Rahman et al., 2003), and typically, the payload motion is modeled as a lumped mass system or mathematical pendulum. Depending on the crane type, various control strategies have been proposed and validated numerically and/or experimentally. Strategies based on H^{∞} (Alfi et al., 2015; Golovin and Palis, 2019), neural network (Xia and Luan, 2015; Ramli et al., 2018),

[1]Shanghai Engineering Research Center of Marine Renewable Energy, Shanghai Ocean University, Shanghai, China
[2]KLA Corporation, Milpitas, CA, USA
[3]School of Production Engineering Management, Technical University of Crete, Greece
[4]School of Mechanical and Power Engineering, Zhengzhou University, Zhengzhou, China
[5]ISVR, University of Southampton, Southampton, UK

Received: 30 May 2022; revised: 6 October 2022; accepted: 3 November 2022

Corresponding author:
Yu Wu, Shanghai Engineering Research Center of Marine Renewable Energy, Shanghai Ocean University, No. 999, Hucheng Ring Road, Nanhui New Town, Pudong New Area, Shanghai 201306, China.
Email: y_wu@shou.edu.cn

nonlinear control (Sun et al., 2018a, 2019; Wu et al., 2020b), adaptive and input shaping control (Qian et al., 2019; Maghsoudi et al., 2019; Zhao and Huang, 2019; Khorshid et al., 2021), optimal control (Sun et al., 2018b; Wu et al., 2020a), vision control (Okubanjo et al., 2018), sliding and saturated control (Tuan and Lee, 2018; Zhang et al., 2020; Aboserre and El-Badawy, 2021), PD control (Zhang et al., 2019), hoisting control (Miranda-Colorado and Aguilar, 2019; Yurchenko and Alevras, 2014), and combination of some of the above strategies (Ramli et al., 2020; Abdullahi et al., 2020) were investigated and presented in the literature. The review papers Hyla (2012); Ramli et al. (2017) comprehensively cover the existing literature up to 2017, whereas the textbook Hong and Shah (2019) published in 2019 also has a number of recent and important references. There are other active control strategies considered, including a mass moving along the pendulum (Iourtchenko, 2006; Maia et al., 2014; Ruta et al., 2019) and passive absorbers (Ibrahim, 2008; Xu et al., 2019; Sarigul-Klijn et al., 2006). Nevertheless, the development of an effective control strategy relies on the information from various sensors essential for decision making. However, in many practical applications, these sensors are not available and cannot be retrofitted; moreover, they can fail leaving a crane operator to deal with the swinging payload alone.

Recently, the authors proposed to use a pendulum tuned mass damper (PTMD) as a potential nonlinear energy absorbing mechanism similar to a tuned mass damper (TMD) (Den Hartog, 2013; Yurchenko, 2014; Lopez et al., 2014; Li and Zhang, 2020). Typically, a TMD is implemented by adding a secondary mass to the original oscillatory single-degree-of-freedom system with a primary mass, where the mass and the stiffness of the TMD are selected or tuned appropriately. In contrary, the PTMD tuning is not obvious since its dynamics is inherently nonlinear and its response frequency depends on the response amplitude. Moreover, the PTMD's natural frequency depends on the pendulum length and thus cannot be selected arbitrary due to the potential spatial constraints, if any. In Yurchenko et al. (2021), the authors studied 3 different options of using PTMD and found that due to the unique properties of the tri-pendulum design, it was very effective in vibration mitigation of the primary mass.

However, in Yurchenko et al. (2021), the authors studied a quasi-static case, where the primary mass was stationary or moving very slowly. Often a pendulum has been used together with another mass–spring system to study autoparametric vibrations and autoparametric absorbers (Hatwal, 1982; Cuvalci and Ertas, 1996; Vazquez-Gonzalez and Silva-Navarro, 2008; Alevras et al., 2014; Gumus and Ertas, 2016). It should be stressed that these studies were focused on developing a pendulum absorber for stationary vibrating linear and nonlinear mass–spring systems, whereas the authors of Yurchenko et al. (2021) have been focused on application of the pendulum absorber to another pendulum. Fuzzy control approach has been applied to a variable length pendulum in Li et al. (2022); in Chen and Sun (2022), a feedback control strategy for a 5-DOF crane system was studied.

In this paper, the authors study a single-degree-of-freedom pendulum subjected to a periodic excitation. Although such an excitation does not realistically act on a crane's payload, it is an important benchmark case to understand the performance of a nonlinear absorber in the non-stationary case of variable length of the primary mass. The authors believe that the proposed methodology when validated can be extended to more realistic excitations, such as impulse or ramp unit, as well as stochastic input. The tri-pendulum nonlinear absorber, which behaves as another pendulum with independently adjustable natural frequency and viscous damping, is applied to the primary mass to study its effectiveness, while the primary pendulum is being lifted up or down. The main motivation is to understand how efficient the earlier proposed by Yurchenko et al.'s (2021) vibration mitigation strategy will be on a reeling up pendulum since it is well-known that a classical TMD is not very effective in non-stationary cases. Moreover, we proposed a novel tuning strategy, which is based on the reeling speed and acceleration, which is known in advance as the properties of the reeling motor, thereby completely excluding the need for any feedback control. In Section 2, the governing equations of motion are derived using the Lagrange approach. Section 3 studies the performance of the nonlinear absorber and the behavior of the primary mass using 2D maps, contracted in the absorber's parameters' space. These maps help to qualitatively understand the dependence of the absorber performance based on its set of parameters. Section 4 proposes to use the surrogate optimization approach to tune the absorber based on the given winch's velocity and acceleration properties only, without any active control or dependence on a system's current state. The numerical results of the optimization within a bounded set of absorber's parameters are presented and discussed. The conclusions are presented in the last section of the paper.

2. The governing equations of motion

The tri-pendulum (Alevras and Yurchenko, 2013) is a special case of the N-pendulum with three separate arms, with lumped masses M_i placed at distance h_i from the center, separated in plane with 120° from each other, and connected to a common hub placed on a bearing to allow oscillating around its suspension point.

Assume that the primary mass is externally excited, as shown in Figure 1(a), and the tri-pendulum is added

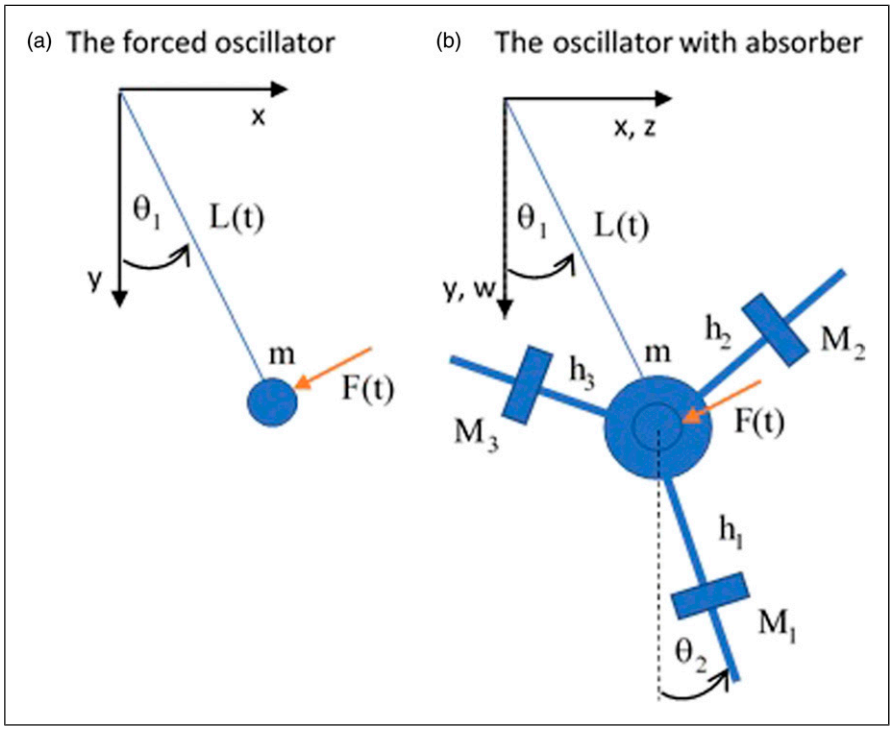

Figure 1. The primary mass with the tri-pendulum absorber.

to this system, creating a two-degree-of-freedom system, as sketched in Figure 1(b). These oscillations may take place when the primary mass is long, like a part of a wind tower, and thus, the proposed study will not cover this case. Let angles θ_1 and θ_2 be the inclination angles of the primary mass m and the tri-pendulum masses M_i, respectively. Then, the geometrical components of the primary mass can be expressed in the Cartesian coordinate system as following

$$\begin{aligned} x_1 &= L\sin\theta_1, & y_1 &= L\cos\theta_1, \\ \dot{x}_1 &= \dot{L}\sin\theta_1 + L\dot{\theta}_1\cos\theta_1, & \dot{y}_1 &= \dot{L}\cos\theta_1 - L\dot{\theta}_1\sin\theta_1, \end{aligned} \tag{1}$$

where $L = L(t)$. The displacement components of each mass of the tri-pendulum can be written as following

$$\begin{aligned} &z_1 = L\sin\theta_1 + h_1\sin\theta_2,\ w_1 = L\cos\theta_1 + h_1\cos\theta_2, \\ &z_2 = L\sin\theta_1 + h_2\cos(\theta_2 + \pi/6),\ w_2 = L\cos\theta_1 \\ &- h_2\sin(\theta_2 + \pi/6), z_3 = L\sin\theta_1 - h_3\cos(\theta_2 - \pi/6), \\ &w_3 = L\cos\theta_1 + h_3\sin(\theta_2 - \pi/6), \end{aligned} \tag{2}$$

The kinetic energy of the system, assuming that $M_1 = M_2 = M_3 = M$ (for the sake of tuning simplicity), $h_2 = h_3$, and $h_1 > h_2$, is given by

$$\begin{aligned} T &= \frac{m}{2}\left(\dot{x}_1^2 + \dot{y}_1^2\right) + \frac{M}{2}\left(\dot{z}_1^2 + \dot{w}_1^2 + \dot{z}_2^2 + \dot{w}_2^2 + \dot{z}_3^2 + \dot{w}_3^2\right) \\ &= \frac{m+3M}{2}\left(\dot{L}^2 + L^2\dot{\theta}_1^2\right) + \frac{M}{2}\left(h_1^2 + 2h_2^2\right)\dot{\theta}_2{}^2 \\ &\quad + ML\dot{\theta}_1\dot{\theta}_2(h_1 - h_2)\cos(\theta_1 - \theta_2) \\ &\quad + M\dot{L}\dot{\theta}_2(h_1 - h_2)\sin(\theta_1 - \theta_2). \end{aligned} \tag{3}$$

The system potential energy is

$$\begin{aligned} U &= (m+3M)gL(1 - \cos\theta_1) + Mg\{h_1[1 - \cos\theta_2] \\ &\quad + h_2[\sin(\theta_2 + \pi/6) - \sin(\pi/6)] - h_3[\sin(\pi/6) \\ &\quad - \sin(\pi/6 - \theta_2)]\} == (m+3M)gL(1 - \cos\theta_1) \\ &\quad + Mg(1 - \cos\theta_2)(h_1 - h_2). \end{aligned} \tag{4}$$

where g is the acceleration of gravity. Then, following the Lagrange equation derivations, the equations of motion are

$$\begin{cases} (m+3M)\left[L^2\ddot{\theta}_1+2L\dot{L}\dot{\theta}_1+Lg\sin\theta_1\right]+ML\Delta h\ddot{\theta}_2\cos(\theta_1-\theta_2)+ \\ ML\Delta h\dot{\theta}_2^2\sin(\theta_1-\theta_2)+c_1\dot{\theta}_1+c_2(\dot{\theta}_1-\dot{\theta}_2)=-F(t)L, \\ M\left[h_1^2+2h_2^2\right]\ddot{\theta}_2+M\Delta h\Big(2\dot{L}\dot{\theta}_1\cos(\theta_1-\theta_2)+L\ddot{\theta}_1\cos(\theta_1-\theta_2)- \\ L\dot{\theta}_1^2\sin(\theta_1-\theta_2)+\ddot{L}\sin(\theta_1-\theta_2)+g\sin\theta_2\Big)+c_2(\dot{\theta}_2-\dot{\theta}_1)=0, \Delta h=h_1-h_2 \end{cases} \tag{5}$$

where c_1 and c_2 are linear damping coefficients and $F(t) = \lambda_1 \cos(\omega t)$. It should be stressed that the viscous damping in the primary mass c_1 was used to avoid introducing other nonlinear effects due to contact that can distort the tuned absorber effect studied in the paper. The viscous friction in the tri-pendulum c_2 can be introduced at the hub during the design stage and can be adjusted accordingly. Introducing the following non-dimensional parameters

$$\mu=\frac{M}{m+3M},\ \gamma=\frac{h_1}{h_2},\ \eta=\frac{L}{h_2},\ \lambda=\frac{\lambda_1}{m+3M},\quad d_1=\frac{c_1}{m+3M},\ d_2=\frac{c_2}{M} \tag{6}$$

equation (5) can be written as (we neglect the term with c_2 in the first equation assuming $c_2/(m + 3M) \ll 1$ for large m)

$$\begin{cases} \ddot{\theta}_1+\mu\dfrac{\gamma-1}{\eta}\ddot{\theta}_2\cos(\theta_1-\theta_2)=-2\dfrac{\dot{L}}{L}\dot{\theta}_1-\mu\dfrac{\gamma-1}{\eta}\dot{\theta}_2^2 \\ \sin(\theta_1-\theta_2)-\Omega_1^2\sin\theta_1-\dfrac{d_1}{L^2}\dot{\theta}_1-\dfrac{\lambda}{L}\cos(\omega t),\ddot{\theta}_2 \\ +\dfrac{\eta(\gamma-1)}{\gamma^2+2}\ddot{\theta}_1\cos(\theta_1-\theta_2)=-\dfrac{\eta(\gamma-1)}{\gamma^2+2} \\ \left[2\dfrac{\dot{L}}{L}\dot{\theta}_1\cos(\theta_1-\theta_2)-\dot{\theta}_1^2\sin(\theta_1-\theta_2)+\dfrac{\ddot{L}}{L}\sin(\theta_1-\theta_2)\right. \\ \left.+\Omega_1^2\sin\theta_2+\dfrac{d_2\eta}{L^2(\gamma-1)}\left(\dot{\theta}_2-\dot{\theta}_1\right)\right],\Omega_1^2=g/L(t) \end{cases} \tag{7}$$

Rewriting equation (7) in the form

$$\begin{cases} \ddot{\theta}_1+\mu\dfrac{\gamma-1}{\eta}\ddot{\theta}_2\cos(\theta_1-\theta_2)=G_2\left(\theta_1,\dot{\theta}_1,\theta_2,\dot{\theta}_2,L,\dot{L},\ddot{L}\right), \\ \ddot{\theta}_2+\dfrac{\eta(\gamma-1)}{\gamma^2+2}\ddot{\theta}_1\cos(\theta_1-\theta_2)=G_1\left(\theta_1,\dot{\theta}_1,\theta_2,\dot{\theta}_2,L,\dot{L},\ddot{L}\right), \end{cases} \tag{8}$$

where functions $G_2 = G_2(\theta_1, \dot{\theta}_1, \theta_2, \dot{\theta}_2, L, \dot{L}, \ddot{L})$ and $G_1 = G_1(\theta_1, \dot{\theta}_1, \theta_2, \dot{\theta}_2, L, \dot{L}, \ddot{L})$ represent the right-hand side (RHS) of the top and bottom equations in (7) correspondingly. Let J be

$$J=1-\mu\frac{(\gamma-1)^2}{\gamma^2+2}\cos^2(\theta_1-\theta_2) \tag{9}$$

one can rewrite equation (8) as

$$\begin{cases} \ddot{\theta}_1=\dfrac{1}{J}\left[G_1-G_2\mu\dfrac{\gamma-1}{\eta}\cos(\theta_1-\theta_2)\right], \\ \ddot{\theta}_2=\dfrac{1}{J}\left[G_2-G_1\dfrac{\eta(\gamma-1)}{\gamma^2+2}\cos(\theta_1-\theta_2)\right]. \end{cases} \tag{10}$$

It should be stressed that the use of approximate analytical methods requires that the RHS of (9) is proportional to a small parameter. As a result, an analytical approach will average the nonlinear effects, practically hiding or losing some of them partially or fully. The genuine interest of this paper is to study the nonlinear interaction of both pendulums when their response angles are relatively large and their behavior is truly nonlinear. Thus, it is reasonable to study such nonlinear effects using a numerical analysis, which is appropriate to capture various nonlinear phenomena that occur in the system. In Table 1, the parameters and variables are presented.

From the practical point of view, one of the most interesting cases is when the primary mass is moving with a constant velocity. Thus, it is reasonable to assume that in the case of a constant velocity, the length of the pendulum will be changing as $L = L_0 + vt$, where L_0 is the initial position of the cable, $v = \dot{L}$ and $a = \dot{v} = 0$. To understand the influence of the accelerating primary mass, another case is considered in this paper, namely, when the primary mass is being moved with a constant acceleration and deceleration, that is, $a = \ddot{L} = const$. It is worth to note that M, h_1, h_2, and d_2 are the absorber parameters, which can be tuned to minimize the swinging of the primary mass.

2.1. Dynamic response of the primary mass with the tri-pendulum absorber

The presented equation of motion (10) can be solved numerically; however, because of the varying primary mass length, its natural frequency will vary. In this study, it is assumed that the cable's length varies between 1 meter and 10 meters with a given speed or a given acceleration. This

Table 1. Parameters and variables of the system.

Parameters/Variables	Meaning
θ_1 and θ_2	Angular position of the primary and tri-pendulum masses
m, M_1, M_2, and M_3	Mass of the primary and tri-pendulum masses
h_1, h_2, and h_3	Distance to the tri-pendulum masses; optimization parameters
$L(t)$, $\dot{L}(t)$, and $\ddot{L}(t)$	Length, velocity, and acceleration of the primary mass
c_1, c_2, d_1, and d_2	Original and normalized viscous damping coefficients
Ω_1	Variable natural frequency of the primary mass
μ, γ, and η	Non-dimensional parameters according to (6)
λ_1 and ω	Excitation amplitude and frequency
g	Acceleration of gravity

interval identifies the undesirable excitation frequency range that is approximately ranging from 0.99 rad/s to 3.13 rad/s. In all the presented simulations, the overall time domain was defined by the velocity of the primary mass from the initial cable length to its final position; thus, the higher the cable velocity, the shorter the computational time.

Figure 2 presents four maps of the numerical results generated for $\omega = 1.1$ rad/s, $\lambda = 0.1$ m, $\mu = 0.03$, and zero initial conditions. The maps in the $\gamma - h_2$ space are presented for three different values of the lifting-up velocities and the values of the damping coefficient $d_2 = 0.1\ m^2/s$ and $d_2 = 0.3\ m^2/s$ in the left and the right columns correspondingly.

The first row corresponds to $v = 0.01$ m/s and the second corresponds to $v = 0.02$ m/s. In these maps, the difference between $\kappa = \max|X_{wa}| - \max|X_a|$ is plotted, where X_a and X_{wa} are the horizontal displacements of the primary mass with and without absorber correspondingly, which are defined according to (1). Here, the values of γ and h_2 corresponding to the warm colors provide significant vibration mitigation and the yellow region can be called the *maximum suppression region*, whereas the cold colors show that the absorber is not very effective. In fact, one can see that in some cases, the vibrations of the primary mass with the absorber can be greater than that without the absorber, as can be seen to the right from the yellow region in some maps. To understand the behavior of the system near and to the right from this region, Figure 3 presents the cut at $\gamma = 3.1$ level for different values of damping d_2 as a function of h_2. It can be observed that with decrease of the damping coefficient d_2, the change between the yellow and dark blue regions becomes steeper, demonstrating the effect of the damping d_2.

A typical time history of the system is presented in Figure 4, where the parameters of the system are taken the same as in Figure 2(a), but at different points on the map. Blue color represents the primary mass response without the absorber, whereas the red color represents the primary mass response with the absorber. Vibration mitigation effect of the absorber can be seen from Figure 4(a) to Figure 4(b). It can be seen from Figure 4(b) that the response amplitude of the primary mass with the absorber is reduced more than twice with the proper values of the parameters. It should be stressed that higher values of these parameters correspond to longer arms of the tri-pendulum, which may be not very practical.

Figure 5 demonstrates the influence of μ on the primary mass response for $\omega = 1.1$ rad/sec, $\lambda = 0.1$ m, and $v = 0.01$ m/s. As expected, one can see that with the increase of the absorber mass from $\mu = 0.01$ to $\mu = 0.05$, its effectiveness is improved. While the maximum suppression region is gradually widening from Figure 5(a) to Figure 5(b), it remains in the same position with respect to the horizontal axis. In Figure 6, one can observe an opposite trend of shrinking of that region with its gradual shifting to the left with the increase of ω.

To provide a fair comparison of the accelerating primary mass to the previous case, it is assumed that the system will have a contact acceleration/deceleration. Under the assumption that these two intervals of acceleration and deceleration are equal in time, it is possible to derive the relationship between the mean velocity of the primary mass, its acceleration, and the primary pendulum length difference between the initial and final positions for the lifting-up operation

$$< v > = \frac{\sqrt{a(L_o - L_f)}}{2}, \quad L_0 > L_f \tag{11}$$

where $< v > = - < \dot{L} >$ is the mean lifting-up velocity and $a = \ddot{L}$ is the acceleration. This equation is used to select an acceleration value, which will result in the same time of the lifting-up process. Figure 7 presents the map in $\gamma - h_2$ space for $< v > = 0.05$ m/s and the primary mass moving up with a constant acceleration/deceleration. Numerical results have also indicated that the increase of μ leads to higher vibration suppression; however, the peak values move to the right to higher values of h_2. The regions with the negative effect of the absorber grow bigger indicating again the adverse effect of the speed.

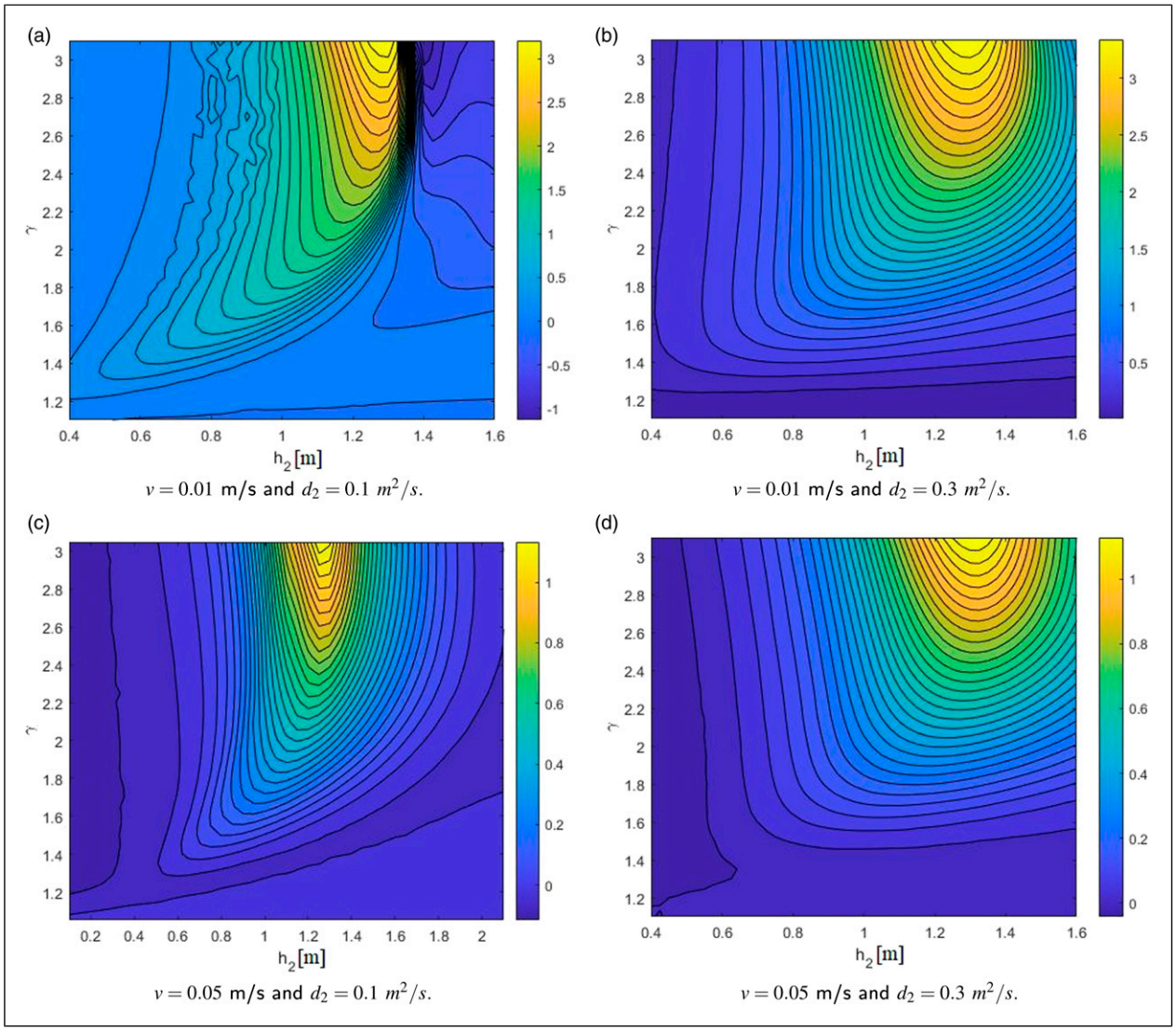

Figure 2. Values of κ for different v and d_2 and λ = 0.1 m, ω = 1.1 rad/sec, and μ = 0.03.

3. Optimization of the absorber performance

3.1. Optimization approach

As it has been demonstrated above, the tri-pendulum nonlinear absorber can effectively mitigate the primary mass vibrations in some cases. The purpose of this work is to implement a passive absorber, which neither requires any active control nor embedded sensors. In this case, it is believed that the excellent strategy would be to tune the absorber parameters based on the winch operating properties, that is, the winch's velocity and acceleration only. It can be done by studying the response of the system for a given set of initial conditions, the system and excitation parameters, and then optimizing the systems' response to provide the best overall result.

The goal is to find the tri-pendulum distances h_1 and h_2 (within given ranges) that minimize the mean oscillation energy of the primary mass. The objective function is specified as follows.

First, we take the sum of the corresponding terms in the representations of the kinetic and potential energies (3) and (4) and divide them by $m + 3M$ for convenience, deriving the normalized energy of the primary mass

$$H = gL(1 - \cos\theta_1) + \frac{1}{2}L^2\dot{\theta}_1^2 \tag{12}$$

The term with $\dot{L}^2$ from (3) is not included since it relates to the energy of ascending/descending primary mass, rather than its vibrations. Next, we consider the mean of (12) over the time interval $[0, t_f]$ such that the boundary conditions $L(0) = L_0$ and $L(t_f) = L_f$ are satisfied

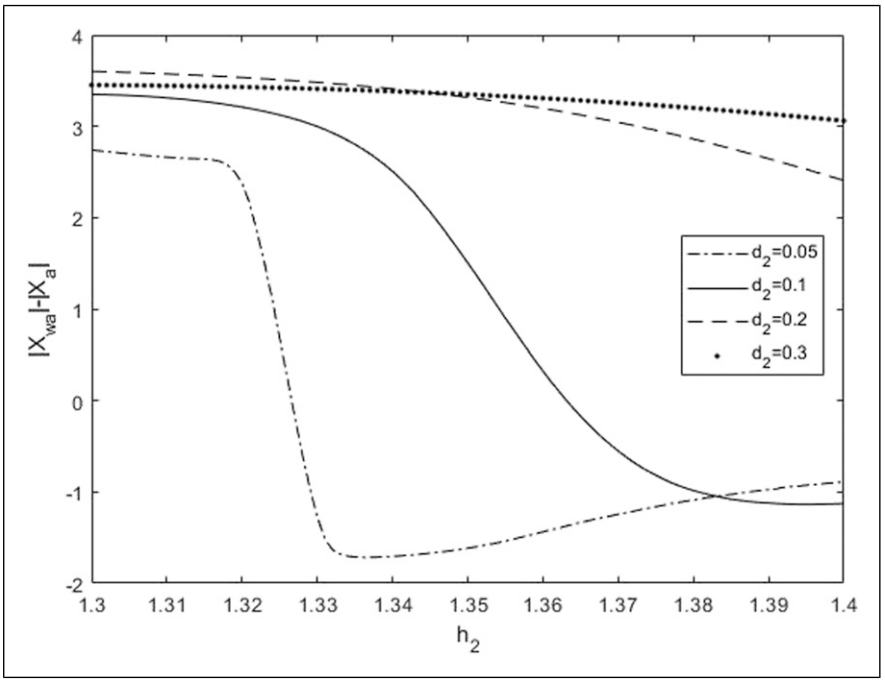

Figure 3. The difference in horizontal displacement κ for γ = 3.1 and v = 0.01 m/s.

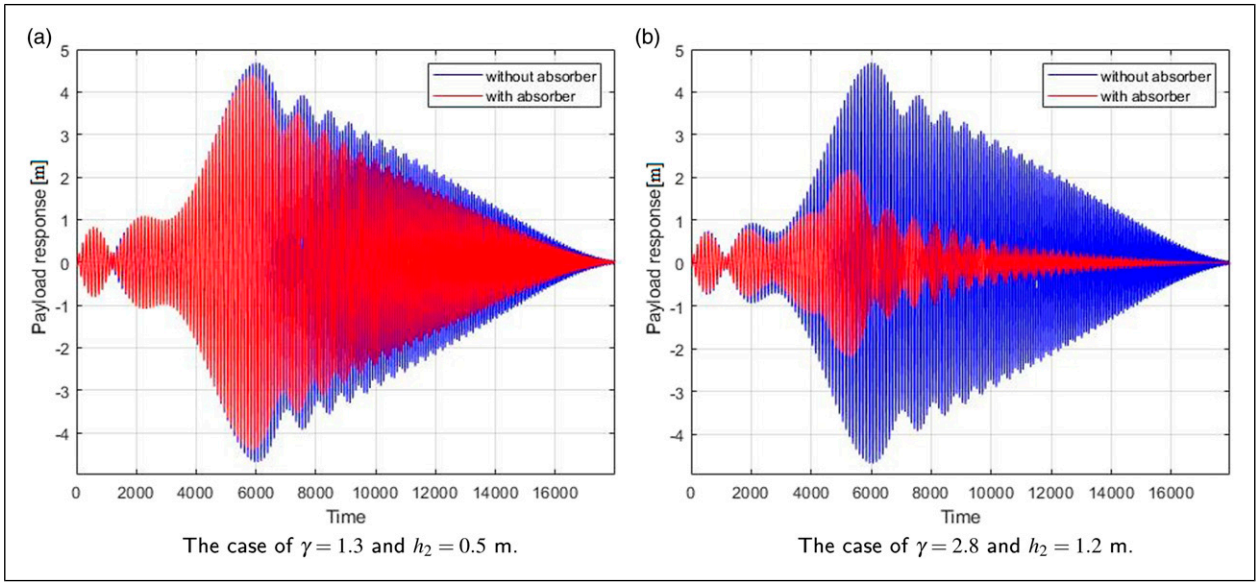

Figure 4. Time history of the primary mass horizontal displacement [m] for λ = 0.1 m, ω = 1.1 rad/sec, μ = 0.03, d_2 = 0.1 m^2/s, v = 0.01 m/s, and different values of γ and h_2.

$$\frac{1}{t_f}\int_0^{t_f}\left(gL(t)(1-\cos\theta_1(t))+\frac{1}{2}L^2(t)\dot{\theta}_1^2(t)\right)\mathrm{d}t \qquad (13)$$

It is also noted that the actual values of the external force parameters λ and ω and initial states $\overline{\theta}(0)=(\theta_1(0),\dot{\theta}_1(0),\theta_2(0),\dot{\theta}_2(0))$ (obviously affecting the system dynamics) may not be known in a particular setting. It is hence reasonable to determine the objective function by averaging the mean energy (13) over some finite grid within certain ranges of λ, ω, and $\overline{\theta}(0)$ (in Yegorov (Egorov) et al., 2021), the advantages of such an averaging approach are demonstrated as applied to a somewhat different class of damping problems). It is

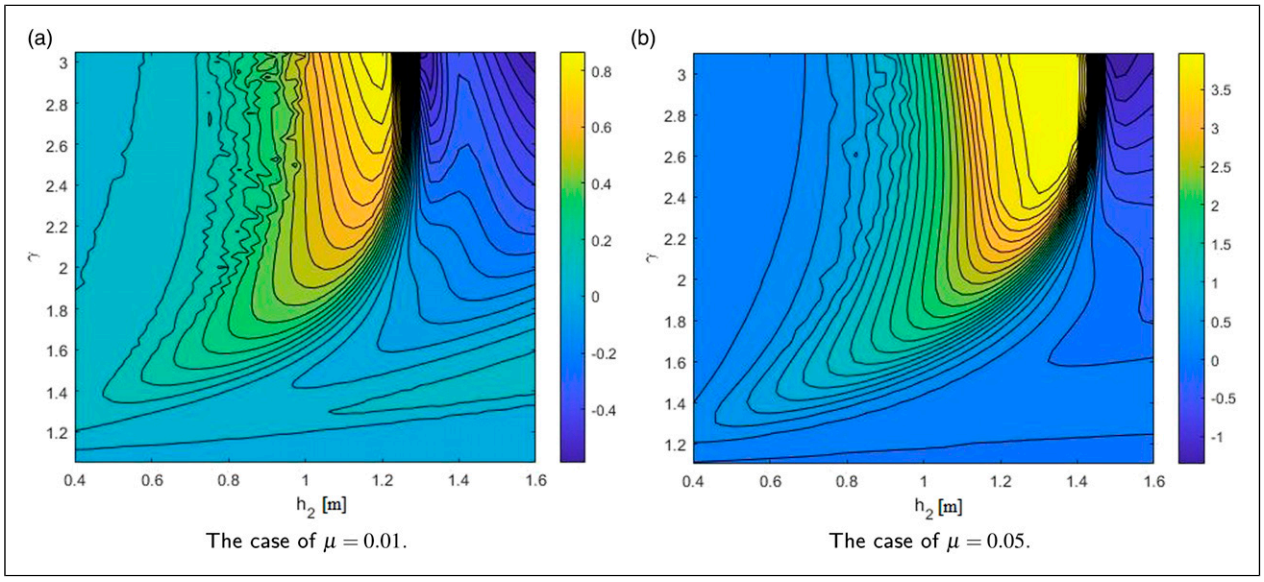

Figure 5. Difference in the horizontal response of the primary mass κ for different values of μ and λ = 0.1 m, ω = 1.1 rad/sec, d_2 = 0.1 m^2/s, and v = 0.01 m/s.

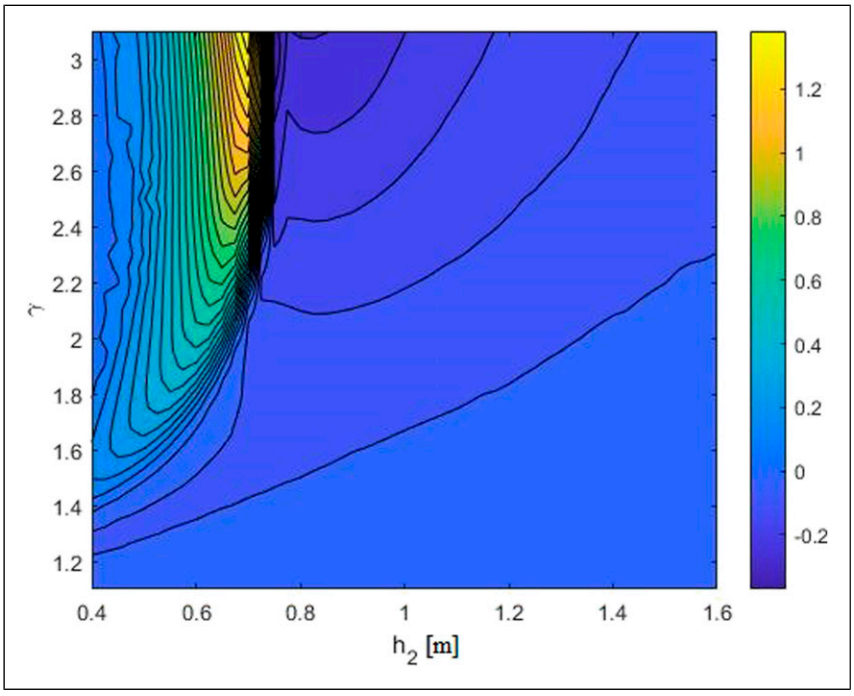

Figure 6. Difference in the horizontal response of the primary mass κ for λ = 0.1 m, d_2 = 0.1, and v = 0.01 m/s.

proposed to construct the grid from a limited number of quasi–Monte Carlo nodes. In general, quasi–Monte Carlo grids reduce the clamping of standard Monte Carlo grids, which is critical to high-dimensional problems, and can rely on Halton, Sobol, or Faure quasi-random number sequences (Kocis and Whiten, 1997; Chilan and Conway, 2019).

The main idea of surrogate optimization is to work with relatively simple interpolation or regression models built from objective function values at a limited number of

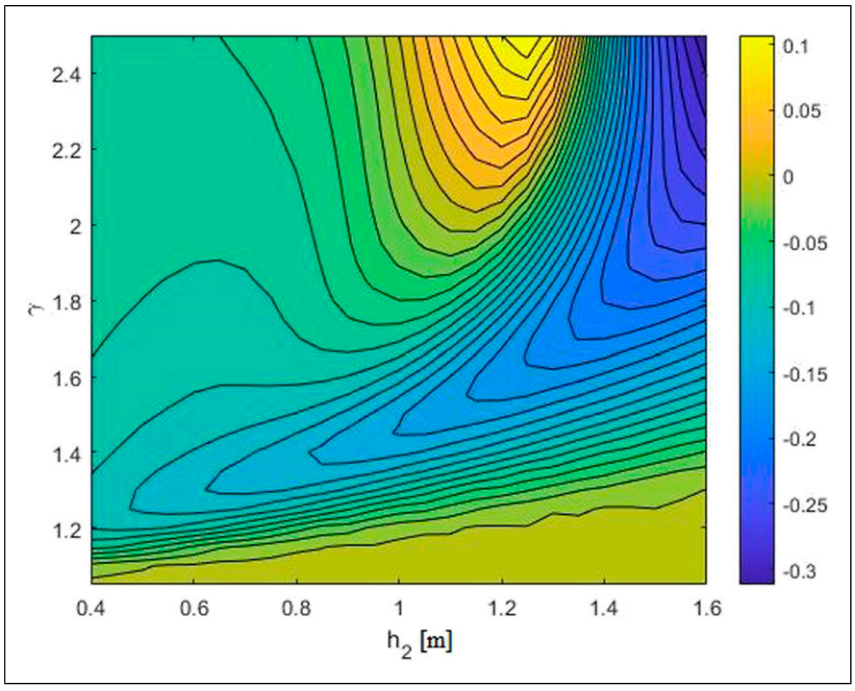

Figure 7. Difference in the horizontal response of the primary mass κ for $<v> = 0.05$ m/s, $\mu = 0.01$, $\lambda = 0.1$ m, $\omega = 1.1$ rad/sec, and $d_2 = 0.1\ m^2/s$.

sample points and update these models iteratively (Gutmann, 1999; Koziel and Leifsson, 2016). Such fast computable approximations of an objective function are called surrogates. For example, the corresponding implementation in the MATLAB Global Optimization Toolbox MathWorks© (2022) involves radial basis function interpolation for surrogate construction. The optimization algorithm searches for a global extremum and alternates between two stages. The first stage generates or updates a surrogate, while the second stage performs global optimization via the current surrogate, using Kriging algorithm (Chilan and Conway, 2019; Press et al., 2007).

For numerical simulations in this paper, we take

$$L_0 = 10\,m, \quad L_f = 1m, \quad \mu = 0.03 \tag{14}$$

and set the following bounds for h_1 and h_2

$$0.1 \leqslant h_2 \leqslant 1, \quad h_2 < h_1 \leqslant 1.5 \tag{15}$$

Values in (15) are taken to keep the tri-pendulum of relatively reasonable size so that at its maximum values, $h_2 = 1$ m, whereas $h_1 = 1.5$ m. It should be stressed that the condition $h_1 > h_2$ is imposed here to be consistent with the simulations conducted in the previous part. In fact, h_1 may in principle be smaller than h_2, and in this case, the bottom equilibrium position of the tri-pendulum will be unstable while the top equilibrium will become stable.

The mean energy (13) was averaged over a Halton quasi–Monte Carlo grid consisting of 100 nodes in the six-dimensional cuboid given by

$$\lambda \in [0.05, 0.1], \quad \omega \in [0.9, 1.3], \overline{\theta}(0) = \overline{\theta}(0) \in [-0.3, 0.3] \times [-0.3, 0.3] \times [-0.3, 0.3] \times [-0.3, 0.3]. \tag{16}$$

The associated optimal distances h_1 and h_2 would probably not be the best for particular values from λ, ω, and $\overline{\theta}(0)$, but the average performance would certainly be superior.

4. Numerical simulations

A set of the numerical optimizations is performed for the case of the primary mass constant lifting-up speed, a fixed set of parameters without an averaging and with an averaged procedure over the specified above range of parameters λ, ω, and $\overline{\theta}(0)$. Figure 8(a) demonstrates the optimal values of h_1 and h_2 for these two cases, where the without-averaging case was studied for zero initial conditions, $\lambda = 0.08$, $\omega = 1.1$, and $d_2 = 0.1\ m^2/s$. It should be stressed that one can observe peaks for h_1 parameter at every grid point. These oscillations are direct result of Kriging interpolation, which has been selected due to its high performance and smoothing properties.

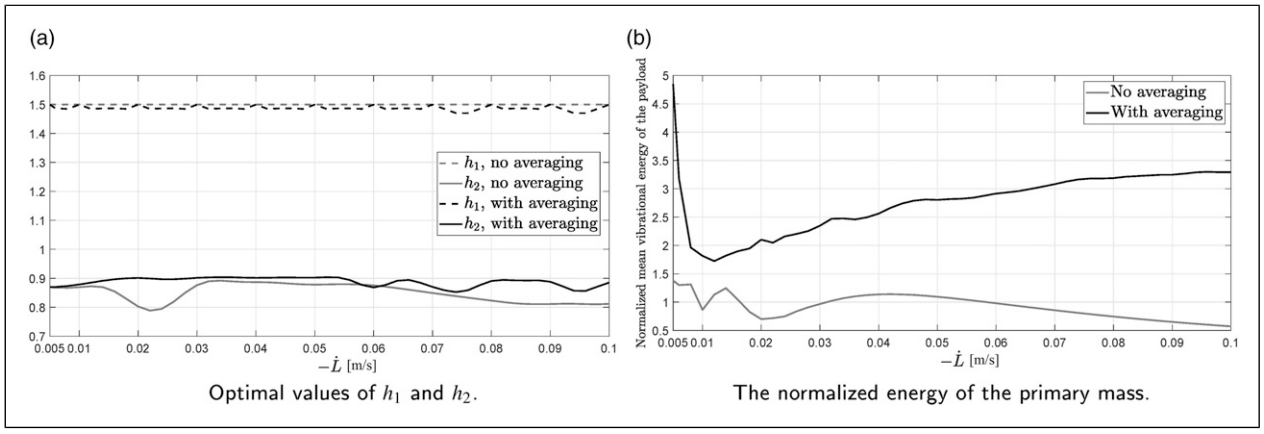

Figure 8. The case of a constant lifting-up speed.

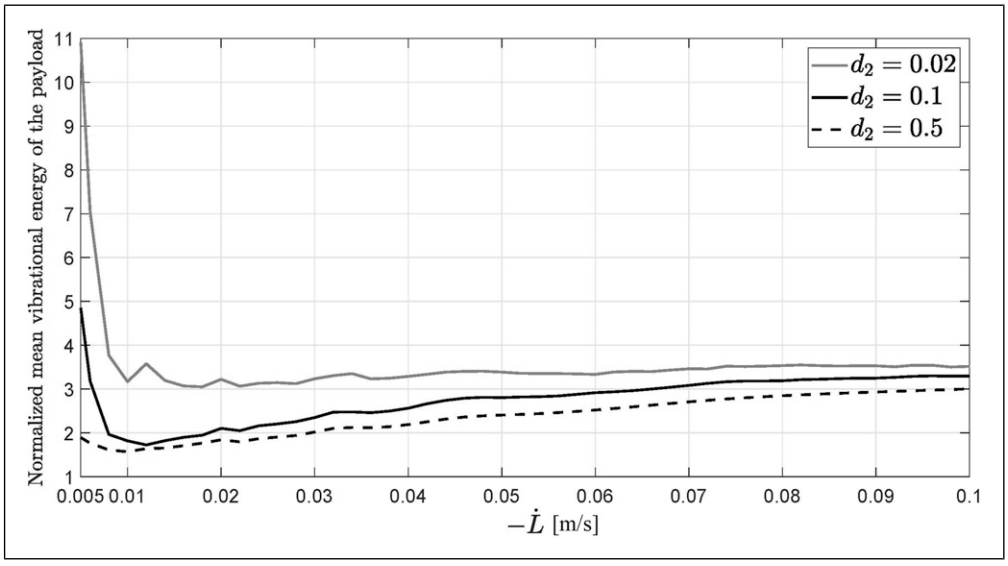

Figure 9. The optimal values of the normalized primary mass energy as a function of the lifting velocity averaged over λ, ω, $\overline{\theta}(0)$, and different values of the damping coefficient d_2.

It can be seen in Figure 8(a) that over the presented range of the lifting velocities, the optimal values of h_1 are almost the same; however, there is some difference in the optimal values of h_2 for some values of the lifting-up velocity. For instance, the difference in the optimal values of h_2 can be observed when $v = 0.02$ m/s. Figure 8(b) demonstrates the graphs of the primary mass normalized energy as a function of the primary mass velocity for the two cases as in Figure 8(a) and optimal values of h_1 and h_2.

Figure 9 presents the results of the optimization for the case of the constant lifting-up velocity and different values of the absorber damping d_2. It can be observed from Figure 9 that there is a significant difference in the results of the normalized primary mass energy near the very slow or quasi-static values of the lifting-up velocity.

Next set of figures demonstrates the results of the optimization for the case of the accelerating and decelerating primary mass according to (11). Figure 10(a) demonstrates the results of the optimization for the optimal values of h_1 and h_2, where h_1 is suggested to remain the same. However, the optimal value of h_2 becomes very low, around 0.2 m, when the mean speed goes above 0.06 m/s, although for the lower values of the mean velocities, the situation is different.

Figure 10(b) presents the results of the normalized energy of the primary mass as a function of mean velocity for different values of the absorber damping averaged over the range of λ, ω, and $\overline{\theta}(0)$. The lowest values are achieved

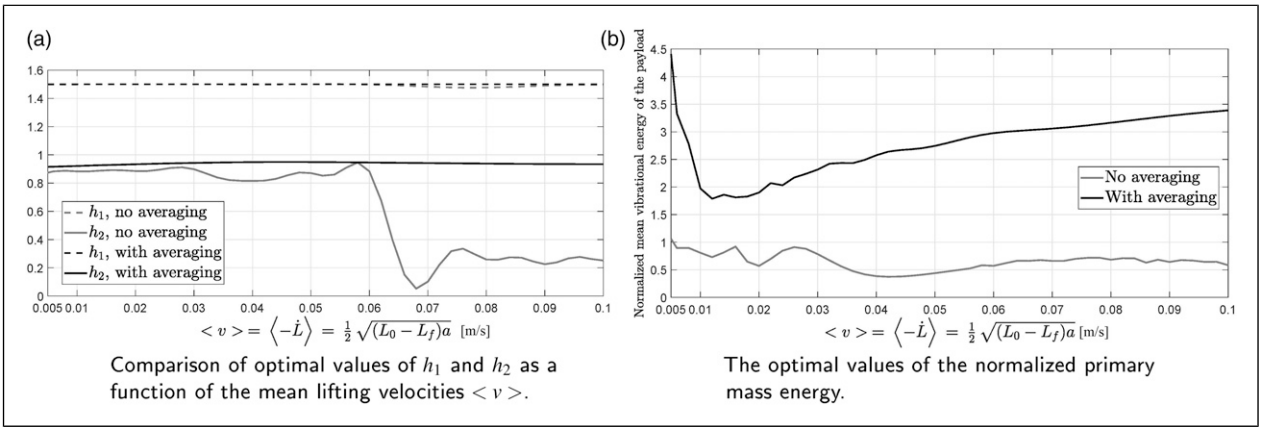

Comparison of optimal values of h_1 and h_2 as a function of the mean lifting velocities $< v >$.

The optimal values of the normalized primary mass energy.

Figure 10. The case of constant acceleration/deceleration of the primary mass.

around $< v > = 0.015$m/s tending to the same value of normalized energy as in Figure 9 at higher values of the mean velocity.

5. Conclusion

In this work, a tri-pendulum nonlinear absorber was proposed to mitigate vibrations of the primary lumped mass pendulum. The lifting motion of the primary mass, with either a given speed or a given acceleration/deceleration, was accounted for by introducing a time-dependent pendulum's length. 2D maps constructed in the $\gamma - h_2$ space have shown the performance of the absorber based on the selected values of the system's parameters. It has been shown that the maps have a prominent suppression region, where the vibrations of the primary mass are mitigated substantially. However, there are regions where the vibration suppression is not significant or the absorber has a negative effect on the primary mass, resulting in a larger response amplitude of the latter. These investigations have also demonstrated the following effect of the system's parameters:

- the larger the lifting velocity of the primary mass, the lower the vibration mitigation effect of the tri-pendulum absorber;
- the higher the damping of the tri-pendulum, the wider the maximum suppression region; however, it also moves up to larger values of γ;
- the larger the mass ratio, the better the vibration mitigation performance of the absorber; and
- the longer the absorber arms, the higher the effect of vibration mitigation.

Using the surrogate optimization approach, we have studied the absorber performance within a reasonable restricted set of the absorber parameters, namely, the arm lengths. The numerical results have been obtained for a fixed set of the initial conditions as well as by averaging over some set of these parameters. The numerical results of the optimization have demonstrated excellent performance of the nonlinear absorber when it is tuned. Moreover, the paper has demonstrated the feasibility of the proposed tuning strategy, which does not require any active control at all.

Acknowledgement

This work is supported by the Fishery Engineering and Equipment Innovation Team of Shanghai High-level Local University.

Declaration of conflicting interests

The author(s) declared no potential conflicts of interest with respect to the research, authorship, and/or publication of this article.

Funding

The author(s) received no financial support for the research, authorship, and/or publication of this article.

ORCID iD

Yu Wu https://orcid.org/0000-0001-9619-1654

References

Abdel-Rahman EM, Nayfeh AH and Masoud ZN (2003) Dynamics and control of cranes: a review. *Journal of Vibration and Control* 9(7): 863–908.

Abdullahi AM, Mohamed Z, Hea S, et al. (2020) Efficient control of a 3d overhead crane with simultaneous payload hoisting and wind disturbance: design, simulation and experiment. *Mechanical Systems and Signal Processing* 145: 106893.

Aboserre LT and El-Badawy AA (2021) Robust integral sliding mode control of tower cranes. *Journal of Vibration and Control* 27(9–10): 1171–1183.

Alevras P, Bobryk R and Yurchenko D (2014) Stability of an autoparametric pendulum system with impacts. *Journal of Sound and Vibration* 333(26): 7233–7247.

Alevras P and Yurchenko D (2013) Dynamics of the n-pendulum and its application to a wave energy converter concept. *International Journal of Dynamics and Control* 1: 290–299.

Alfi A, Shokrzadeh A and Asadi M (2015) Reliability analysis of h-infinity control for a container ship in way-point tracking. *Applied Ocean Research* 52: 309–316.

Chen H and Sun N (2022) An output feedback approach for regulation of 5-dof offshore cranes with ship yaw and roll perturbations. *IEEE Transactions on Industrial Electronics* 69(2): 1705–1716.

Chilan C and Conway B (2019) Optimal nonlinear control using Hamilton–Jacobi–bellman viscosity solutions on unstructured grids. *Journal of Guidance, Control, and Dynamics* 43: 1–9.

Cuvalci O and Ertas A (1996) Pendulum as vibration absorber for flexible structures: experiments and theory. *Journal of Vibration and Acoustics* 118(4): 558–566.

Den Hartog J (2013) *Mechanical Vibrations*. New York: Courier Dover Publications.

Golovin I and Palis S (2019) Robust control for active damping of elastic gantry crane vibrations. *Mechanical Systems and Signal Processing* 121: 264–278.

Gumus E and Ertas A (2016) Analysis of free pendulum vibration absorber using flexible multi-body dynamics. *Shock and Vibration* 2016: 1–19.

Gutmann HM (1999) A radial basis function method for global optimization. *Journal of Global Optimization* 19: 201–227.

Hatwal H (1982) Notes on an autoparametric vibration absorber. *Journal of Sound and Vibration* 83(3): 440–443.

Hong KS and Shah UH (2019) *Dynamics and Control of Industrial Cranes*. Singapore: Springer Singapore.

Hyla P (2012) The crane control systems: a survey. In: 2012 17th International Conference on Methods Models in Automation Robotics (MMAR), Miedzyzdroje, Poland, 2012, pp. 505–509.

Ibrahim RA (2008) Recent advances in nonlinear passive vibration isolators. *Journal of Sound and Vibration* 314(3): 371–452.

Iourtchenko DV (2006) Random vibrations of swings. *Journal of Sound and Vibration* 292(3): 1011–1014.

Khorshid E, Al-Fadhli A, Kea A, et al. (2021) Command shaping with reduced maneuvering time for crane control. *Journal of Vibration and Control* 27(11–12): 1311–1323.

Kocis L and Whiten WJ (1997) Computational investigations of low-discrepancy sequences. *ACM Trans. Math. Softw* 23(2): 266–294.

Koziel S and Leifsson L (2016) *Introduction to Surrogate Modeling and Surrogate-Based Optimization*. Cham: Springer International Publishing, pp. 31–61.

Li LY and Zhang T (2020) Analytical analysis for the design of nonlinear tuned mass damper. *Journal of Vibration and Control* 26(9–10): 646–658.

Li M, Chen H and Zhang R (2022) An input dead zones considered adaptive fuzzy control approach for double pendulum cranes with variable rope lengths. *IEEE* 27: 1–12.

Lopez R, Miguel L and Beck A (2014) Tuned mass dampers for passive control of structures under Earthquake excitations. In: *Encyclopedia of Earthquake Engineering*. Cham: Springer, pp. 1–12.

Maghsoudi MJ, Ramli L, Sea S, et al. (2019) Improved unity magnitude input shaping scheme for sway control of an underactuated 3d overhead crane with hoisting. *Mechanical Systems and Signal Processing* 123: 466–482.

Maia N, Gandino E, Sea M, et al. (2014) Damping effects induced by a mass moving along a pendulum. *Shock and Vibration* 2014: 1–9.

MathWorks© (2022) *Matlab Global Optimization Toolbox Documentation*. URL https://www.mathworks.com/help/gads

Miranda-Colorado R and Aguilar LT (2019) A family of anti-swing motion controllers for 2d-cranes with load hoisting/lowering. *Mechanical Systems and Signal Processing* 133: 106253.

Okubanjo A, Oluwadamilola O and Adekomaya O (2018) Vision based control of gantry crane system. *Anadolu University Journal of Science and Technology-A Applied Sciences and Engineering* 19: 1023–1032.

Press WH, Teukolsky SA and Wea V (2007) *Numerical Recipes: The Art of Scientific Computing*. New York: Cambridge University Press.

Qian Y, Fang Y and Lu B (2019) Adaptive robust tracking control for an offshore ship-mounted crane subject to unmatched sea wave disturbances. *Mechanical Systems and Signal Processing* 114: 556–570.

Ramli L, Mohamed Z, Abdullahi AM, et al. (2017) Control strategies for crane systems: a comprehensive review. *Mechanical Systems and Signal Processing* 95: 1–23.

Ramli L, Mohamed Z, Mea E, et al. (2020) Efficient swing control of an overhead crane with simultaneous payload hoisting and external disturbances. *Mechanical Systems and Signal Processing* 135: 106326.

Ramli L, Mohamed Z and Jaafar HI (2018) A neural network-based input shaping for swing suppression of an overhead crane under payload hoisting and mass variations. *Mechanical Systems and Signal Processing* 107: 484–501.

Ruta G, Li C, Zhang Z, et al. (2019) An improved principle of rapid oscillation suppression of a pendulum by a controllable moving mass: Theory and simulation. *Shock and Vibration* 2019: 1–11.

Sarigul-Klijn N, Lopez I, Sarigul-Klijn M, et al. (2006) Vibration mitigation using passive active tunable (PAT) system: Experimental Aspects. *Journal of Vibration and Acoustics* 129(2): 209–216.

Sun N, Fang Y, Chen H, et al. (2018a) Nonlinear antiswing control of offshore cranes with unknown parameters and persistent ship-induced perturbations: Theoretical design and hardware experiments. *IEEE Transactions on Industrial Electronics* 65(3): 2629–2641.

Sun N, Wu Y, Chen H, et al. (2018b) An energy-optimal solution for transportation control of cranes with double pendulum dynamics: design and experiments. *Mechanical Systems and Signal Processing* 102: 87–101.

Sun N, Wu Y, Liang X, et al. (2019) Nonlinear stable transportation control for double-pendulum shipboard cranes with ship-motion-induced disturbances. *IEEE Transactions on Industrial Electronics* 66(12): 9467–9479.

Tuan LA and Lee SG (2018) Modeling and advanced sliding mode controls of crawler cranes considering wire rope elasticity and complicated operations. *Mechanical Systems and Signal Processing* 103: 250–263.

Vazquez-Gonzalez B and Silva-Navarro G (2008) Evaluation of the autoparametric pendulum vibration absorber for a duffing system. *Shock and Vibration* 15: 355–368.

Wu Q, Wang X, Lea H, et al. (2020a) Dynamic analysis and time optimal anti-swing control of double pendulum bridge crane with distributed mass beams. *Mechanical Systems and Signal Processing* 144: 106968.

Wu X, Xu K and He X (2020b) Disturbance-observer-based nonlinear control for overhead cranes subject to uncertain disturbances. *Mechanical Systems and Signal Processing* 139: 106631.

Xia G and Luan T (2015) Study of ship heading control using rbf neural network. *International Journal of Control and Automation* 8: 227–236.

Xu ZD, Chen ZH, Huang XH, et al. (2019) Recent advances in multi-dimensional vibration mitigation materials and devices. *Frontiers in Materials* 6: 00143.

Yegorov (Egorov) I, Uden A and Yurchenko D (2021) Optimal performance comparison of nonlinear energy sinks and linear tuned mass dampers. In: *ASME 2021 International Design Engineering Technical Conferences and Computers and Information in Engineering Conference*. New York, NY: ASME.

Yurchenko D (2014) *Tuned Mass and Parametric Pendulum Dampers under Seismic Vibrations*. Berlin, Heidelberg: Springer Berlin Heidelberg, pp. 1–22.

Yurchenko D and Alevras P (2014) Stability, control and reliability of a ship crane payload motion. *Probabilistic Engineering Mechanics* 38: 173–179.

Yurchenko D, Alevras P, Zhou S, et al. (2021) Nonlinear vibration mitigation of a crane's payload using pendulum absorber. *Mechanical Systems and Signal Processing* 156: 107558.

Zhang M, Zhang Y, Chen H, et al. (2019) Model-independent pd-smc method with payload swing suppression for 3d overhead crane systems. *Mechanical Systems and Signal Processing* 129: 381–393.

Zhang S, He X, Zhu H, et al. (2020) Partially saturated coupled-dissipation control for underactuated overhead cranes. *Mechanical Systems and Signal Processing* 136: 106449.

Zhao X and Huang J (2019) Distributed-mass payload dynamics and control of dual cranes undergoing planar motions. *Mechanical Systems and Signal Processing* 126: 636–648.